1   **The breakdown of static and evolutionary allometries during climatic upheaval**

2   Anieke Brombacher[1*], Paul A. Wilson[1], Ian Bailey[2], Thomas H.G. Ezard[1,3]

3

4   [1]National Oceanography Centre Southampton, University of Southampton, Waterfront

5   Campus, European Way, Southampton SO14 3ZH, UK

6   [2]Camborne School of Mines and Environmental Sustainability Institute, University of

7   Exeter, Penryn Campus, Cornwall TR10 9FE, UK

8   [3]Centre for Biological Sciences, University of Southampton, Life Sciences Building 85,

9   Highfield Campus, Southampton SO17 1BJ, UK

10   [*]Corresponding author. Email: j.brombacher@noc.soton.ac.uk

11

14

15   **Abstract**

16   The influence of within-species variation and covariation on evolutionary patterns is

17   well established for generational and macroevolutionary processes, most prominently

18   through genetic lines of least resistance. However, it is not known whether intraspecific

19   phenotypic variation also directs microevolutionary trajectories into the long term

20   when a species is subject to varying environmental conditions. Here we present a

21   continuous, high-resolution bivariate record of size and shape changes among 12,633

22   individual planktonic foraminifera of a surviving and an extinct-going species over 500

23   thousand years. This time interval spans the late Pliocene to earliest Pleistocene

24   intensification of Northern Hemisphere glaciation, an interval of profound climate

25   upheaval that can be divided into three phases of increasing glacial intensity. We found

26   that within each of these three Plio-Pleistocene climate phases the within-population

27   allometries predict evolutionary change from one time-step to the next, and that the

28   within-phase among-population (i.e. evolutionary) allometries match their

29   corresponding static (within-population) allometries. However, the evolutionary

30   allometry across the three climate phases deviates significantly from the static and

31   phase-specific evolutionary allometries in the extinct-going species. Although

32   intraspecific variation leaves a clear signature on mean evolutionary change from one

33   time-step to the next, our study suggests that the link between intraspecific variation

34   and longer-term micro- and macroevolutionary phenomena is prone to environmental

35   perturbation that can overcome constraints induced by within-species trait covariation.

36

Introduction

Intraspecific variation is essential for evolution. Phenotypic variation is the target for natural selection, with the possibilities for phenotypic change determined by the extent of genetic variation. Many traits do not evolve independently: selection on one trait can influence the response to selection in others (Lande 1979; Lande and Arnold 1983). These constraints among traits can have large impacts on the direction of evolution, either facilitating evolution in the case of positive covariances (Gavrilets and Losos 2009), or constraining adaptation when covariances are negative (Agrawal and Stinchcombe 2009). Lande (1979) used a multivariate quantitative genetics framework to describe brain: body size allometry in mammals. From one generation to the next, the multivariate Breeder's equation (Lande 1979) predicts the change in mean n-dimensional phenotypes as:

$$\mathbf{z} = \mathbf{G}\beta \qquad (1)$$

Here $\mathbf{z}$ is an n-dimensional vector representing the change in n trait means, $\mathbf{G}$ is the additive genetic variance-covariance matrix with genetic variances on the diagonal elements and covariances as non-diagonal elements, and β is an n-dimensional vector consisting of directional selection gradients (Lande 1979; Lande and Arnold 1983). Repeated over many generations, the phenotype is expected to evolve in the direction of the dominant eigenvector of $\mathbf{G}$, which has been defined as the line of least genetic resistance $\mathbf{g_{max}}$ (Schluter 1996). Although populations have been shown to evolve along lines of least resistance on generational time scales (Lande 1979; Lande and Arnold 1983; Bégin et al. 2003), as well as among modern species and genera (Lande 1979; Schluter 1996), we lack robust data on how trait covariance evolves along species branches in deep time.

64   Allometries present specific examples of trait covariations, with a given trait covarying

65   with body size according to a power relationship (Huxley 1932). They are considered

66   exemplary lines of least evolutionary resistance (Pélabon et al. 2014) because allometric

67   constraints imply that internal growth regulators restrict trait evolution. Marroig and

68   Cheverud (2005) showed that the direction of evolutionary change in New World

69   Monkeys mainly occurred along within-population allometric slopes of body size and

70   cranial features, using morphological data of extant species supplemented by modelled

71   reconstructions of ancestral morphology. One of the challenges to empirical studies of

72   how trait covariance evolves in free-living populations, and an explanation for the

73   "dismally few" empirical tests (Estes and Arnold 2007), is that studies using recent

74   species are restricted to a comparison of relatively few matrices on contemporaneous

75   populations (Arnold et al. 2008). Empirical studies of phenotypic change over long time

76   scales require the fossil record, which typically lacks genetic information. Quantitative

77   morphological traits represent a multi-locus representation of intraspecific variation,

78   and have been shown to influence adaptive evolution (Simpson 1953). Over long

79   timescales, assuming a constant selection regime (Arnold et al. 2008) (and mutational

80   pleiotropy notwithstanding (Cheverud 1996)), evolutionary constraints due to

81   phenotypic trait covariation provide a good approximation of the adaptive landscape

82   (Arnold et al. 2001). While pleiotropy is often present in mutation input, this

83   observation implies that it is instructive to study changes in the relationships among

84   traits.

85

86   Hunt (2007) and Renaud et al. (2006) applied the concept of Schluter's (1996) lines of

87   least resistance to the fossil record. Hunt (2007) found that speciation in an ostracode

88   clade spanning ~37 Myrs tended to occur in the direction of maximum phenotypic

89   variation of the ancestor population. Renaud et al. (2006) showed that dental patterns in

90   rodents were channelled along the direction of greatest intraspecific variation over an

91   11 Myr-interval. Additionally, Haber (2016) showed that traits evolve fastest if

92   divergence is aligned with the phenotypic covariance matrix in ruminant skulls.

93   Phylogenetic comparative methods have identified changing trait covariance as a key

94   diagnostic among distinct subclades during the origin of birds (Puttick et al. 2014).

95   These four studies focus on changing trait covariances on macroevolutionary time

96   scales, but no observations have been reported of how trait covariance evolves during a

97   species' existence.

98

99   The allometric constraint hypothesis states that within-population allometries typically

100 remain constant, shaping evolutionary constraints over longer time scales (Pélabon et

101 al. 2014). Firmat et al. (2014) showed that static (within-population) allometries predict

102 evolutionary (i.e. among-species) allometries on <1 million-year time scales, implying

103 consistent alignment between **G** and the adaptive landscape (Lande 1980; Cheverud

104 1984; Arnold 1992). However, a shift in evolutionary optima would upset this

105 alignment, forcing the individuals and population into an alternative selective regime.

106 Under such a displaced optimum (Estes and Arnold 2007), the consistency between

107 within-population and evolutionary allometries might be expected to break down.

108 Renaud et al. (2006) reported that among-species morphological variation in one of

109 their two studied lineages departed from the lines of least resistance following

110 pronounced environmental change. Their sampling resolution, however, did not allow

111 for the analysis of the evolution of static allometries within species over time.

112 Additionally, Hunt (2007) showed that evolution in an ostracode clade did follow the

113 lines of least resistance initially, but the effect eroded after a few million years. To study

114 changes in static allometries as a response to changing selective gradients and their

115 effect on evolutionary allometries, high-temporal resolution records of individual

116 species are needed.

117

118   Here, we analyse size and shape allometries from 12,633 individuals in two ecologically

119   and environmentally similar planktonic foraminifera species found at Integrated Ocean

120   Drilling Program (IODP) Site U1313 (~41° N) situated in the mid-latitude North Atlantic

121   Ocean. Planktonic foraminifera are sexually reproducing protists distributed in high

122   abundance throughout the world's oceans. The large population size, global distribution

123   and excellent preservation potential of their calcite shells make them uniquely suited for

124   continuous, high-resolution morphological reconstructions over millions of years. We

125   explore the temporal consistency of allometries within and among populations during

126   the most recent great climate transition in Earth's history: the late Pliocene to earliest

127   Pleistocene intensification of Northern Hemisphere glaciation (iNHG) (Mudelsee and

128   Raymo 2005). We investigate two main questions. First, do allometric lines of least

129   phenotypic resistance predict evolutionary change within species over thousands of

130   generations? Second, do within-population (static) and among-species (evolutionary)

131   allometries become decoupled during climate upheaval?

132

133   **Material & Methods**

134   **Study species**

135   We focus on two ecologically similar species, *Truncorotalia crassaformis* and

136   *Globoconella puncticulata* (Figure 1, 2 (inserts)), characterised by low trochospiral tests

137   with flattened spiral sides, inflated umbilical sides and umbilical-extraumbilical

138   apertures (Kennett and Srinivasan 1983). Both inhabit similar habitats with highest

139   abundances in thermocline waters at middle and low latitudes (Kennett and Srinivasan

140   1983; Aze et al. 2011). *T. crassaformis* originated around 5.7 Ma and survives to the

141   present day. *G. puncticulata* first appeared around 4.6 Ma and became extinct at 2.41 Ma

142   (Wei 1994b), shortly after the onset of significant Northern Hemisphere glaciation at

143   2.72 Ma (Bailey et al. 2013). Wei (1994a) has reported allometric changes in the *G.*

144   *puncticulata* lineage on macroevolutionary time scales. In particular, he noted that *G.*

145 *puncticulata* gave rise to its only descendant species, *G. inflata,* through shifts in

146 ontogenetic allometric relationships starting around 3.5 Ma in the southwest Pacific

147 (Wei 1994a; Wei 1994b). *G. inflata* did not occur in the North Atlantic until ~2.09 Ma

148 (Berggren et al. 1995; Chapman et al. 1998), ~30,000 years after the extinction of *G.*

149 *puncticulata*. The planktonic foraminifera biostratigraphy of Site U1313 reports no

150 overlap between the local stratigraphic ranges of *G. puncticulata* and *G. inflata* (Channell

151 et al. 2006) and no individuals of *G. inflata* were found in our higher resolution sample

152 set of the study's target time interval. The extirpation of *G. puncticulata* from the North

153 Atlantic is therefore not attributable to replacement by a descendant species.

154

155 **Material**

156 IODP Site U1313 is located in the mid North Atlantic Ocean at the base of the upper

157 western flank of the Mid-Atlantic Ridge at a water depth of 3426 m (41 °N, 32.5 'W), at

158 the northern edge of the North Atlantic Gyre. In this oceanographic environment,

159 surface currents are driven by clockwise wind circulation in the high-pressure system

160 overlying the subtropical North Atlantic. Deflected by the Coriolis force, these currents

161 form a basin-wide rotating circulation system with little movement of surface water

162 currents into or out of the gyre, preventing large-scale migration of plankton and

163 generating a well-mixed eco-evolutionary system. Site U1313 was drilled during IODP

164 Expedition 306 in 2005 and constitutes a reoccupation of Deep Sea Drilling Project

165 (DSDP) Site 607 (Raymo et al. 1990; Channell et al. 2006) using advanced piston coring

166 techniques to provide continuous records of evolutionary change (Channell et al. 2006).

167 The Site U1313 record is characterised by consistently high sedimentation rates (~5

168 cm/kyr) for the past 5 Myr (Lisiecki and Raymo 2005; Channell et al. 2006), a

169 demonstrably continuous record of sedimentation for iNHG (Bolton et al. 2010) and

170 exceptionally well-preserved microfossil carbonate (Lang et al. 2014).

171

172 The time interval studied here spans 2.4 to 2.9 Ma and captures the intensification of

173 Northern Hemisphere Glaciation (iNHG). We identify three distinct climate states in the

174 studied interval characterised by stepwise increases in glacial state in the face of

175 constant interglacial (background) conditions (Figure 2E,F). Before Marine Isotope

176 Stage (MIS) G6 at 2.72 Ma, here called the Initial Phase, Northern Hemisphere ice sheets,

177 as tracked by benthic foraminiferal oxygen isotopes ($\delta^{18}O$), were small (Lisiecki and

178 Raymo 2005; Mudelsee and Raymo 2005). From MIS G6 onwards Northern Hemisphere

179 climate became dominated by 41-kyr glacial-interglacial cycles (here called the

180 Transition Phase, 2.54-2.72 Ma), but glacial ice sheets did not reach their full iNHG size

181 until 2.54 Ma with Marine Isotope Stages 96, 98 and 100 (Bailey et al. 2013) (here called

182 the Glacial Phase, <2.54 Ma). By comparing within-population allometries to

183 evolutionary allometries within these three climate phases, as well as over the entire

184 study interval, we are able to provide new insights into the evolution of allometric

185 relationships during times of global climatic upheaval.

186

187 We used 75 of the samples at every ~30 cm (~5-kyr-resolution) from the shipboard

188 primary splice studied originally by Bolton et al. (2010): 20 samples in the Initial Phase,

189 30 in the Transition Phase and 25 in the Glacial Phase. The site's average bioturbation

190 depth is estimated to be 2-3 cm (Channell et al. 2006) implying no time averaging of

191 foraminifera populations between consecutive samples. For age control, we used the

192 orbital-resolution benthic foraminiferal $\delta^{18}O$ stratigraphy for Site U1313 generated by

193 Bolton et al. (2010). The samples were dry-sieved over a >150 μm^2 mesh sieve and split

194 using a microsplitter until a single split contained 70-150 specimens of *T. crassaformis*

195 or *G. puncticulata*. The splits were picked for all specimens of both of these species,

196 resulting in a total of 12,629 specimens (6058 specimens of *T. crassaformis* and 6575 of

197 *G. puncticulata*) over the studied interval. While picking for *T. crassaformis* extra care

198 was taken to exclude specimens from the closely related and morphologically similar

species *Truncorotalia oceanica*, *Truncorotalia ronda*, *Truncorotalia viola* and *Truncorotalia hessi* (Kennett and Srinivasan 1983; Stewart 2003). Foraminifera shells were mounted on glass slides in groups of 20 individuals using double-sided adhesive tape with the apertures facing upwards. Groups were imaged using an Infinity 3 Lumenera camera mounted on an Olympus SZX10 light microscope. Because we aim to evaluate changes in traits as a consequence of climate change, we chose to only analyse traits with known functional morphologies. Shell size is known to reflect a species' ecological optimum (Hecht 1976; Schmidt et al. 2004) and shell shape impacts the test volume to surface area ratio, influencing respiration and metabolic processes (Caromel et al. 2014). Shell area and aspect ratio (the ratio between test height and width) were extracted from the images using an automated image analysis macro in the Image Pro Premier software (Figure 1). To assess measurement consistency a subset of 100 individuals per species was remounted and reanalysed. Measurement errors were defined as the difference between two repeated measurements on the same individual, divided by the mean of those two measurements. Results from both sets of measurements were highly consistent with average trait errors less than 5% (Table S1).

Analysis

The R package 'paleoTS' (Hunt 2006) allows analysis of paleontological time series using maximum likelihood models, which we use to test whether univariate trait evolution in the different climatic states is best described by stasis, directional evolution or a random walk. To test whether trait evolution occurred more slowly than would be consistent with genetic drift, we calculated Lynch's delta metric (Lynch 1990). Given the observed within-population phenotypic variance, this measure decribes the range of evolutionary rates that would be consistent with neutral evolution (10^{-3} - 10^{-5}). Higher values imply directional selection, whereas lower values support hypotheses of stabilising selection. To quantify trait responses to changes in Northern Hemisphere climate we used linear

226   models to compare our morphology records to the LR04 benthic $\delta^{18}O$ stack representing

227   Northern Hemisphere glacial-interglacial climate cycles (Lisiecki and Raymo 2005) after

228   taking first differences to account for temporal autocorrelation and for consistency with

229   the random walk approach of the paleoTS analyses.

230

231   To study trait covariation over time, phenotypic variance-covariance matrices $\mathbf{P_t}$ were

232   constructed using individual measurements of shell size and shape at time t scaled to

233   unit variance to produce measurements in comparable units. The dominant eigenvector

234   of $\mathbf{P_t}$, here called $\mathbf{p_{max}}$, describes maximum phenotypic variation (Schluter 1996; Hunt

235   2007) and, in our case, represents the static allometric size-shape relationship at time t.

236   Evolutionary allometries were calculated in the same way using the sample means of

237   size and shape to reconstruct the variance-covariance matrix over the entire study

238   interval (total evolutionary allometries) as well as from separate climate phases (phase-

239   specific evolutionary allometries). To test whether populations preferentially evolve

240   along static allometries from one time step to the next, we measured the angle θ

241   between $\mathbf{p_{max}}$ at time t and the direction of evolutionary divergence z from the sample

242   mean at time t to the sample mean at time $t+1$ (Figure 3A), and compared θ to a

243   simulated distribution of angles between two randomly chosen vectors generated using

244   Knuth's Algorithm (Knuth 1969). A Wilcoxon rank-sum test was performed to check if

245   the distribution of all θ differed from the randomly generated angles. A set of angles

246   significantly smaller than the randomly generated angles implies that population

247   evolution from one time step to the next is constrained by its within-population

248   allometries. A paired Wilcoxon test was applied to test if both species were similarly

249   constrained by their allometric lines of least resistance.

250

251   Over longer time scales and under a constant selection regime, species are expected to

252   preferentially evolve along $\mathbf{p_{max}}$ (Schluter 1996; Hunt 2007; Firmat et al. 2014; Haber

253   2016), resulting in evolutionary allometries similar to the within-population allometries

254   (Firmat et al. 2014; Voje et al. 2014). To determine whether within-population

255   allometries also predict evolutionary allometries during intervals of global

256   environmental change, we compared the within-population allometries within climate

257   phases to both the phase-specific evolutionary allometries as well as the evolutionary

258   allometry across the entire studied interval (see Figure 3B for an example).

259

Results

Time series of size and shape dynamics in both species are presented in Figure 2A-D. We particularly note an abrupt decrease in size by 30±9% in *G. puncticulata* at the start of the Transition Phase during MIS G6. No significant relationships were found between any of the traits and $\delta^{18}O$ (Linear Model, $p = 0.61$, $R^2 = 0.0037$ and $p = 0.99$, $R^2 = 2.2*10^{-4}$ for size and shape of *G. puncticulata* and $p = 0.64$, $R^2 = 0.0031$ and $p = 0.77$, $R^2 = 0.0012$ for size and shape of for size and shape of *T. crassaformis*, see also Figure 4), arguing against genetic and plastic species response to climate change. Maximum likelihood models implemented in the paleoTS package provide approximately 60-70% support for a directionless random walk as compared to directional evolution (20-30%) or stasis (0-20%) for all time series over the entire studied interval (Table 1). Analysed within separate climate states, size of *G. puncticulata* is best described by stasis in the Initial Phase and by a random walk in the Transition and Glacial phases, whereas shape is best described by stasis in the Initial and Glacial Phases, and by a random walk in the Transition Phase. Size of *T. crassaformis* most resembles a random walk in the Initial and Transition Phases and stasis in the Glacial Phase, while shape is best described by a random walk throughout (Table 1). Additionally, for all studied traits Lynch's delta values fall well outside the 10^{-3} – 10^{-5} range proposed by Lynch (1990) to represent neutral evolution (see Table 2), implying a form of stabilising selection acting on all traits.

T. crassaformis occupies a similar position in size-shape space throughout the studied interval with a strong overlap among the separate climate phases (Figure 5A). Sample means of *G. puncticulata* go from large and square-shaped in the Initial Phase, to decreasing shell area and increasing aspect ratio in the Transition and Glacial Phases, hinting at a strong size: shape allometry in this species (Figure 5B). However, within-population allometries are weak in both species (Figure 5C,D). Visual inspection of the

287   data shows that the within-population allometries of *G. puncticulata* are grouped in their

288   respective climate phases. In *T. crassaformis* the slopes change from weakly positive

289   (Initial Phase) to weakly negative (Transition Phase) to neutral (Glacial Phase). In *G.*

290   *puncticulata* within-population allometries show comparable slopes but different

291   intercepts in the Initial and Glacial phases, with the Transition Phase acting as a bridge

292   between the other two phases with more variable slopes and intercepts.

293

294   The evolutionary allometries within phases follow each phase's set of within-population

295   allometries in both species (Figure 5C,D). For both *T. crassaformis* and *G. puncticulata*

296   the phase- specific evolutionary allometries are significantly different among phases

297   (ANOVA performed on phase-specific evolutionary slopes, $p<0.001$ for both species).

298   The *T. crassaformis* evolutionary allometries shift from weakly positive in the Initial

299   Phase, to weakly negative in the Transition Phase to almost neutral in the Glacial Phase,

300   whereas those in *G. puncticulata* are weakly negative in the Initial and Glacial Phases,

301   and strongly negative during the Transition Phase. Together, the phase-specific

302   allometries explain 5.5% of all variance in *T. crassaformis*, as opposed to 33.6% in *G.*

303   *puncticulata* (ANCOVA performed on phase-specific evolutionary slopes, $p<0.01$ for both

304   species with phase as a categorical explanatory variable, see Table 3). In *T. crassaformis*

305   the evolutionary allometry over the entire studied interval (Figure 5C, black line) is

306   comparable to the species' phase-specific evolutionary allometries ($p<0.01$, see Table 3).

307   *G. puncticulata* on the other hand shows a strong negative slope ($p<0.001$) comparable

308   to the Transition Phase allometry, but in contrast to the evolutionary allometries in the

309   Initial and Glacial Phase and most of the within-population allometries. This allometric

310   breakdown implies that, for this extinct-going species, within-population and short-term

311   evolutionary allometries do not predict long-term allometric trends during times of

312   climatic upheaval.

313

314   The distribution of the angles θ between $\mathbf{p}_{max}$ and the direction of evolutionary

315   divergence $\mathbf{z}$ are significantly smaller than angles drawn from a random distribution for

316   both species (Wilcoxon rank sum test, $p<0.01$ and $p<0.005$ for *G. puncticulata* and *T.*

317   *crassaformis*, respectively; Figure 5, Table 4). Despite their qualitatively different

318   dynamics (Figure 5), the predictability of phenotypic change based on $\mathbf{p}_{max}$ does not

319   differ between the two species (paired Wilcoxon rank sum test, $p=0.78$). When analysed

320   separately the angles within separate climate phases occasionally deviate from this

321   pattern. In *T. crassaformis* the angles in the Initial Phase are not significantly different

322   from the randomly generated angles (Wilcoxon rank sum test, $p=0.58$, Table 4), whereas

323   the angles in both the Transition and Glacial Phase are significantly smaller than

324   expected by chance alone (Wilcoxon rank sum test, $p<0.05$ and $p<0.001$ respectively,

325   Table 4) implying that the predictability of phenotypic change increases after the

326   intensification of Northern Hemisphere glaciation. In *G. puncticulata* the angles θ are

327   significantly smaller than the randomly generated angles in both the Initial and Glacial

328   Phases (Wilcoxon rank sum test, $p<0.05$, Table 4), whereas no significant difference was

329   detected in the Transition Phase (Wilcoxon rank sum test, $p=0.283$, Table 4). θ does not

330   vary systematically with the within-sample size and shape covariance (linear

331   regressions, $p>0.05$), implying that large phenotypic correlations do not increase the

332   predictability of the lines of least resistance.

333

334   **Discussion**

335   **Allometries within climate phases**

336   Despite low within-population (static) allometric slopes, long-term evolutionary change

337   occurs preferentially along the within-population allometric lines of least resistance, a

338   finding which is consistent with results of studies on generational (Schluter 1996) and

339   macroevolutionary time scales (Renaud et al. 2006; Hunt 2007). In *T. crassaformis* the

340   angles θ between the directions of predicted ($\mathbf{p}_{max}$) and observed ($\mathbf{z}$) evolutionary

341   change are significantly smaller than expected by chance, implying that the lines of least

342   resistance, to some extent, predict phenotypic change of this species through time.

343   Traits are best described by a Random Walk (Table 1), and in all cases Lynch's Delta

344   values indicate stabilising selection. It may seem counterintuitive that trait evolution is

345   consistent with both a Random Walk and stabilising selection, but stabilising selection

346   could maintain a population near a non-stationary adaptive peak. Using the divergence

347   data compilation by Gingerich (2001), Estes and Arnold (2007) showed that such a

348   displaced optimum had the highest explanatory power among multiple competing

349   models of phenotypic evolution. If the optimum shifts, stabilising selection will attempt

350   to drag the population towards the new peak (Estes and Arnold 2007). Assuming the

351   optimum shifts according to a Random Walk, we would expect the sample means to

352   oscillate on or close to $\mathbf{p}_{max}$ but with zero net overall change rather than a directional

353   pattern. Note that the random walk models (Table 1) are univariate, whereas we

354   conceptualize each foraminifera as bivariate when testing allometric constraints on the

355   predictability of $\mathbf{p}_{max}$. Within each climate phase the phase-specific evolutionary

356   allometries match the within-population allometries, implying that within-population

357   allometries can predict evolutionary allometries over time-steps spanning ~100,000

358   years. In *G. puncticulata* evolution occurs significantly close to $\mathbf{p}_{max}$ in the Initial and

359   Glacial Phases. However, this pattern breaks down during the Transition Phase when

360   the species' angles between $\mathbf{z}$ and $\mathbf{p}_{max}$ are randomly distributed (Table 4) and the

361   within-population allometric slopes are highly variable (Figure 5D, yellow lines; 4F,

362   yellow bars). In this interval the species shifts from large and square-shaped shells to

363   smaller and more rectangular shells (Figure 5B), resulting in a strongly negative phase-

364   specific evolutionary allometry (Figure 5D, dashed and solid yellow lines).

365

366   The primary reduction in size of *G. puncticulata* occurred during MIS G6, the first major

367   glacial in the Transition Phase. MIS G6 marks the onset of significant widespread

368   glaciation in the Northern Hemisphere (NHG) (Bailey et al. 2013) and a time of profound

369   oceanographic change in the North Atlantic (Naafs et al. 2012; Lang et al. 2016). At Site

370   U1313, sea surface temperature fell by ~6 °C as compared to the preceding interglacial

371   stage (Naafs et al. 2010; Friedrich et al. 2013) and major increases occurred in cold

372   stage (glacial) surface ocean primary productivity and North American-sourced aeolian

373   dust deposition, delivering nutrients to the oligotrophic surface waters of the North

374   Atlantic Subtropical Gyre (Naafs et al. 2012; Lang et al. 2014). It is possible, therefore,

375   that trait response to new environmental pressures over-rode internal evolutionary

376   constraints (Beldade et al. 2002), forcing the fitness peak of the adaptive landscape in

377   morphospace (Arnold et al. 2001) to shift to trait combinations better adapted to glacial

378   environments. The best supported mode of size evolution shifts from Stasis in the Initial

379   Phase to a Random Walk in the Transition Phase, implying that this phenotypic change

380   is driven by a new selection regime in the Transition Phase. Although there may be a

381   role for directional evolution during parts of the Transition Phase, no strong evidence

382   was provided for Directional Selection over the whole interval or within each phase. No

383   significant correlation was detected between *G. puncticulata* size or shape and on-going

384   high-latitude climate approximated by the global benthic $\delta^{18}O$ stack (Lisiecki and Raymo

385   2005) (Figure 4). However, local environmental change associated with iNHG in the

386   surface ocean might have crossed a critical threshold for the species. Planktonic

387   foraminifera species have very specific temperature ranges for optimum growth

388   (Lombard et al. 2009; Lombard et al. 2011) and the decrease in temperature associated

389   with MIS G6 could have reduced the growth potential for *G. puncticulata*. Although

390   climate shifted back to an interglacial state following MIS G6, the decrease in size also

391   meant a loss of maximum size variance because the two covary, and the interglacial

392   environmental conditions did not last long enough for the species to regain their initial

393   maximum size. The species' extinction at 2.41 Ma has been linked to iNHG (Wei 1994a;

394   Chapman et al. 1998; Scott et al. 2007), further pointing to a higher species-specific

395   sensitivity to glacial conditions. However, the impact of global environmental change on

396   the species' extinction remains to be tested among multiple populations living under

397   different environmental conditions.

398

399   The increase in shell aspect ratio and its covariance with size is more challenging to

400   explain. Smaller shell size reduces drag and increases settling velocity through the water

401   column, making it more difficult for individuals to retain their preferred depth habitat.

402   The changes in shell shape necessary to influence settling velocity are nevertheless

403   smaller (5-6% (Caromel et al. 2014)) than the typical intraspecific variation observed

404   (25-50% (Schmidt et al. 2004)), while the settling velocities reported by Caromel et al.

405   (2014) imply that shells would sink below the thermocline in several hours regardless

406   of shape, implying that active buoyancy regulation by the individual determines its

407   position in the water column. Although it is possible that a decrease in mean shell size

408   requires an attendant flattening of shell shape to facilitate maintenance of position in

409   the water column, the covariation between size and shape within samples is often weak,

410   implying limited effects of trait covariation on buoyancy.

411

412   Alternatively, we might hypothesize that the change in population trait means during

413   the Transition Phase reflects widespread migration of morphologically distinct

414   populations. Surface ocean currents in the North Atlantic Ocean are proposed to have

415   undergone major reorganisations from ~2.7 Ma (Naafs et al. 2010). A southward shift of

416   the North Atlantic Current (NAC) could have transported populations of *G. puncticulata*

417   previously restricted to sub-polar regions into the mid latitudes. It has been suggested,

418   based on dinoflagellate assemblage work, that the NAC was deflected south of Site

419   U1313 only from MIS 104 onwards (Hennissen et al. 2014). However, a study of

420   foraminiferal calcite geochemistry proposes that the position of the NAC probably lay

421   well north of Site U1313 during the Late Pliocene to Earliest Pleistocene (Friedrich et al.

422   2013), implying a maintained position of Site U1313 in the North Atlantic Gyre with

423   little changes in surface water currents. Regardless, changes in surface water currents

424   are suggested to have occurred mainly during glacials, with currents returning to

425   previous conditions during interglacials (Naafs et al. 2010). Thus, if migration of

426   morphologically distinct populations of *G. puncticulata* was responsible for the changes

427   in trait means reported here, we would expect to observe alternating changes in

428   morphology tracking the more intense (inter)glacial cycles during the Transition and

429   Glacial Phases and a strong overall correlation between climate and traits, which is not

430   the case (Figure 2C,D, Figure 4).

431

432   **Allometries among climate phases**

433   In *T. crassaformis* the phase-specific evolutionary allometries change from positive in

434   the Initial Phase, to negative in the Transition Phase to almost neutral in the Glacial

435   Phase (Figure 5C). Although all phase groups of evolutionary allometric slopes are

436   significantly different, they are comparable in magnitude. The evolutionary allometry

437   over the entire studied interval corresponds well with the phase-specific evolutionary

438   and within-population allometries, implying that in *T. crassaformis*, within-population

439   allometries predict evolutionary allometries on various time scales, despite pronounced

440   global climate upheaval. In *G. puncticulata* the evolutionary allometries in the Initial and

441   Glacial Phases have similar slopes but different intercepts, with both phases bridged by

442   the stronger negative allometry in the Transition Phase (Figure 5D). However, sample

443   means are characterised by decreasing size and increasing aspect ratios, with largest

444   and most square-shaped shells in the Initial Phase and smallest, most rectangular shells

445   in the Glacial Phase, which is reflected by a strong negative evolutionary allometry over

446   the entire interval. Because the long-term evolutionary allometry deviates from the

447   within-population and phase-specific evolutionary allometries, these results imply that

448   environmental change can override allometric relationships over time.

449

General evolutionary implications

451 Projecting our bivariate size-shape matrices evokes Raup's seminal ammonoid

452 morphospace (1966), which uses trait frequencies as fitness surrogates to provide a

453 good approximation of the adaptive landscape under a consistent selective regime

454 (Arnold et al. 2001). Our time-averaged samples obfuscate generation-by-generation

455 selection estimates by amalgamation, yet do estimate the fitness optimum when the

456 conditions are stable. The predictive ability of the lines of least resistance (Figure 5E,F)

457 infers a non-symmetric ellipsoidal fitness peak, upon which the species oscillates. Our

458 calculations of Lynch's Delta reject drift as the dominant evolutionary mode for both

459 traits in both species. Despite the co-occurrence of the shift in *G. puncticulata* size with

460 the intensification of Northern hemisphere glaciation (Bailey et al. 2013), there is no

461 evidence to suggest that either of our two species evolves on a fine scale in response to

462 Northern hemisphere climate cycles inferred from benthic $\delta^{18}O$. Taken together, these

463 two results imply a role for stabilizing selection either maintaining species location

464 around a fitness peak in the Initial and Glacial phases, or pulling the species towards a

465 "displaced optimum" (Estes and Arnold 2007) during the Transition Phase. The two

466 optima for *G. puncticulata* form an apparent ridge in the evolutionary allometry when

467 viewed across the whole interval (Figure 5D), but this feature is attributable to sampling

468 through heterogeneous environmental conditions and the associated breakdown of

469 within-population and evolutionary allometries among phases. This discrepancy

470 between evolutionary and within-population allometry contrasts with recent results on

471 over 300 animal taxa (Voje et al. 2014) and fossil rodents (Firmat et al. 2014), but

472 neither of these studies sampled through a major climate transition. The phenotypic

473 covariance might be maintained by the evolutionarily constraining mechanisms of

474 allometries (Pélabon et al. 2014), by a particular environmental context, or a

475 combination of both. The generality of when a changing environmental context prompts

476   a reconfiguration of the relationship between within-population and evolutionary

477   allometries remains to be tested across species with different macroevolutionary fates,

478   spatial locations and allometric strengths.

479

480

481   **Conclusion**

482   We show that under constant environmental variability the within-population

483   allometric lines of least resistance predict evolutionary allometries on

484   microevolutionary time scales. However, in one of the studied species the evolutionary

485   allometry shifted away from the within-population allometries across intervals marked

486   by pronounced climate upheaval. We suggest that changed environmental conditions

487   related to the intensification of Northern Hemisphere Glaciation pushed this species off

488   its peak on the adaptive landscape, away from the direction of intraspecific phenotypic

489   variation. Intraspecific variation left a clear signature on evolutionary change from one

490   time-step to the next in both species studied (Figure 5), but the generality of when

491   phenotypic covariance interacts with environmental perturbation, and how this

492   interaction links to longer-term microevolutionary trends and macroevolutionary

493   phenomena, remains to be tested.

494

506 **References**
507
508 Agrawal, A. F., and J. R. Stinchcombe. 2009. How much do genetic covariances alter the

509   rate of adaptation? Proceedings of the Royal Society B: Biological Sciences

510   276:1183-1191.

511 Arnold, S. J. 1992. Constraints on phenotypic evolution. American Naturalist 140:S85-

512   S107.

513 Arnold, S. J., R. Bürger, P. A. Hohenlohe, B. C. Ajie, and A. G. Jones. 2008. Understanding

514   the evolution and stability of the G-matrix. Evolution 62:2451-2461.

515 Arnold, S. J., M. E. Pfrender, and A. G. Jones. 2001. The adaptive landscape as a

516   conceptual bridge between micro-and macroevolution. Genetica 112:9-32.

517 Aze, T., T. H. Ezard, A. Purvis, H. K. Coxall, D. R. Stewart, B. S. Wade, and P. N. Pearson.

518   2011. A phylogeny of Cenozoic macroperforate planktonic foraminifera from

519   fossil data. Biol Rev Camb Philos Soc 86:900-927.

520 Bailey, I., G. M. Hole, G. L. Foster, P. A. Wilson, C. D. Storey, C. N. Trueman, and M. E.

521   Raymo. 2013. An alternative suggestion for the Pliocene onset of major northern

522   hemisphere glaciation based on the geochemical provenance of North Atlantic

523   Ocean ice-rafted debris. Quaternary Science Reviews 75:181-194.

524 Bégin, M., D. A. Roff, and P. Phillips. 2003. The constancy of the G matrix through species

525   divergence and the effects of quantitative genetic constraints on phenotypic

526   evolution: a case study in crickets. Evolution 57:1107-1120.

527 Beldade, P., K. Koops, and P. M. Brakefield. 2002. Developmental constraints versus

528   flexibility in morphological evolution. Nature 416:844-847.

529 Berggren, W.-A., F. Hilgen, C. Langereis, D. V. Kent, J. Obradovich, I. Raffi, M. E. Raymo et

530   al. 1995. Late Neogene chronology: new perspectives in high-resolution

531   stratigraphy. Geological Society of America Bulletin 107:1272-1287.

532   Bolton, C. T., P. A. Wilson, I. Bailey, O. Friedrich, C. J. Beer, J. Becker, S. Baranwal et al.

533   2010. Millennial-scale climate variability in the subpolar North Atlantic Ocean

534   during the late Pliocene. Paleoceanography 25.

535   Caromel, A. G. M., D. N. Schmidt, J. C. Phillips, and E. J. Rayfield. 2014. Hydrodynamic

536   constraints on the evolution and ecology of planktic foraminifera. Marine

537   Micropaleontology 106:69-78.

538   Channell, J. E. T., T. Kanamatsu, T. Sato, R. Stein, C. A. Alvarez Zarikian, M. J. Malone, and

539   Expedition 303/306 Scientists. 2006. Site U1313. Proceedings of the Integrated

540   Ocean Drilling Program 303/306.

541   Chapman, M. R., B. M. Funnell, and P. P. E. Weaver. 1998. Isolation, extinction and

542   migration within Late Pliocene populations of the planktonic foraminiferal

543   lineage Globorotalia (Globoconella) in the North Atlantic. Marine

544   Micropaleontology 33:203-222.

545   Cheverud, J. M. 1984. Quantitative genetics and developmental constraints on evolution

546   by selection. Journal of Theoretical Biology 110:155-171.

547   —. 1996. Developmental integration and the evolution of pleiotropy. American Zoologist

548   36:44-50.

549   Estes, S., and S. J. Arnold. 2007. Resolving the paradox of stasis: models with stabilizing

550   selection explain evolutionary divergence on all timescales. The American

551   Naturalist 169:227-244.

552   Firmat, C., I. Lozano-Fernández, J. Agustí, G. H. Bolstad, G. Cuenca-Bescós, T. F. Hansen,

553   and C. Pélabon. 2014. Walk the line: 600000 years of molar evolution

554   constrained by allometry in the fossil rodent Mimomys savini. Phil. Trans. R. Soc.

555   B 369:20140057.

556   Friedrich, O., P. A. Wilson, C. T. Bolton, C. J. Beer, and R. Schiebel. 2013. Late Pliocene to

557   early Pleistocene changes in the North Atlantic Current and suborbital-scale sea-

558   surface temperature variability. Paleoceanography 28:274-282.

559   Gavrilets, S., and J. B. Losos. 2009. Adaptive radiation: contrasting theory with data.

560   Science 323:732-737.

561   Gingerich, P. D. 2001. Rates of evolution on the time scale of the evolutionary process.

562   Genetica 112:127-144.

563   Haber, A. 2016. Phenotypic Covariation and Morphological Diversification in the

564   Ruminant Skull. The American Naturalist 187:576-591.

565   Hecht, A. D. 1976. An ecologic model for test size variation in recent planktonic

566   foraminifera: applications to the fossil record. Journal of Foraminiferal Research

567   6:295-311.

568   Hennissen, J. A. I., M. J. Head, S. De Schepper, and J. Groeneveld. 2014. Palynological

569   evidence for a southward shift of the North Atlantic Current at ~2.6 Ma during

570   the intensification of late Cenozoic Northern Hemisphere glaciation.

571   Paleoceanography 29:564-580.

572   Hunt, G. 2006. Fitting and comparing models of phyletic evolution: random walks and

573   beyond. Paleobiology 32:578-601.

574   Hunt, G. 2007. Evolutionary divergence in directions of high phenotypic variance in the

575   ostracode genus *Poseidonamicus*. Evolution 61:1560-1576.

576   Huxley, J. 1932, Problems of relative growth. London, Methuen.

577   Kennett, J. P., and M. S. Srinivasan. 1983, Neogene planktonic foraminifera. A

578   phylogenetic atlas. Stroudsburg, Pennsylvania, Hutchinson Ross Publishing

579   Company.

580   Knuth, D. E. 1969, The Art of Computer Programming vol. II Seminumerical Algorithms,

581   v. 2. Boston, USA, Addison-Wesley.

582   Lande, R. 1979. Quantitative genetic analysis of multivariate evolution, applied to

583   brain:body size allometry. Evolution 33:402-416.

584   Lande, R. 1980. Genetic variation and phenotypic evolution during allopatric speciation.

585   American Naturalist 116:463-479.

586   Lande, R., and S. J. Arnold. 1983. The measurement of selection on correlated characters.

587   Evolution 37:1210-1226.

588   Lang, D. C., I. Bailey, P. A. Wilson, C. J. Beer, C. T. Bolton, O. Friedrich, C. Newsam et al.

589   2014. The transition on North America from the warm humid Pliocene to the

590   glaciated Quaternary traced by eolian dust deposition at a benchmark North

591   Atlantic Ocean drill site. Quaternary Science Reviews 93:125-141.

592   Lang, D. C., I. Bailey, P. A. Wilson, T. B. Chalk, G. L. Foster, and M. Gutjahr. 2016.

593   Incursions of southern-sourced water into the deep North Atlantic during late

594   Pliocene glacial intensification. Nature Geoscience 9:375-379.

595   Lisiecki, L. E., and M. E. Raymo. 2005. A Pliocene-Pleistocene stack of 57 globally

596   distributed benthic δ18O records. Paleoceanography 20.

597   Lombard, F., L. Labeyrie, E. Michel, L. Bopp, E. Cortijo, S. Retailleau, H. Howa et al. 2011.

598   Modelling planktic foraminifer growth and distribution using an

599   ecophysiological multi-species approach. Biogeosciences 8:853-873.

600   Lombard, F., L. Labeyrie, E. Michel, H. J. Spero, and D. W. Lea. 2009. Modelling the

601   temperature dependent growth rates of planktic foraminifera. Marine

602   Micropaleontology 70:1-7.

603   Lynch, M. 1990. The rate of morphological evolution in mammals from the standpoint of

604   the neutral expectation. American Naturalist 136:727-741.

605   Marroig, G., and J. M. Cheverud. 2005. Size as a line of least evolutionary resistance: diet

606   and adaptive morphological radiation in New World monkeys. Evolution

607   59:1128-1142.

608   Mudelsee, M., and M. E. Raymo. 2005. Slow dynamics of the Northern Hemisphere

609   glaciation. Paleoceanography 20.

610   Naafs, B. D. A., J. Hefter, G. Acton, G. H. Haug, A. Martínez-Garcia, R. Pancost, and R. Stein.

611   2012. Strengthening of North American dust sources during the late Pliocene

612   (2.7Ma). Earth and Planetary Science Letters 317-318:8-19.

613   Naafs, B. D. A., R. Stein, J. Hefter, N. Khélifi, S. De Schepper, and G. H. Haug. 2010. Late

614   Pliocene changes in the North Atlantic Current. Earth and Planetary Science

615   Letters 298:434-442.

616   Pélabon, C., C. Firmat, G. H. Bolstad, K. L. Voje, D. Houle, J. Cassara, A. L. Rouzic et al.

617   2014. Evolution of morphological allometry. Annals of the New York Academy of

618   Sciences 1320:58-75.

619   Puttick, M. N., G. H. Thomas, and M. J. Benton. 2014. High rates of evolution preceded the

620   origin of birds. Evolution 68:1497-1510.

621   Raup, D. M. 1966. Geometric analysis of shell coiling: general problems. Journal of

622   Paleontology 40:1178-1190.

623   Raymo, M., W. Ruddiman, N. Shackleton, and D. Oppo. 1990. Evolution of Atlantic-Pacific

624   δ 13 C gradients over the last 2.5 my. Earth and Planetary Science Letters

625   97:353-368.

626   Renaud, S., J. C. Auffray, and J. Michaux. 2006. Conserved phenotypic variation patterns,

627   evolution along lines of least resistance, and departure due to selection in fossil

628   rodents. Evolution 60:1701-1717.

629   Schluter, D. 1996. Adaptive radiation along genetic lines of least resistence. Evolution

630   50:1766 - 1774.

631   Schmidt, D. N., S. Renaud, J. Bollmann, R. Schiebel, and H. R. Thierstein. 2004. Size

632   distribution of Holocene planktic foraminifer assemblages: biogeography,

633   ecology and adaptation. Marine Micropaleontology 50:319-338.

634   Scott, G. H., J. P. Kennett, K. J. Wilson, and B. W. Hayward. 2007. *Globorotalia*

635   *puncticulata*: Population divergence, dispersal and extinction related to

636   Pliocene–Quaternary water masses. Marine Micropaleontology 62:235-253.

637   Simpson, G. G. 1953. The Baldwin effect. Evolution 7:110-117.

638   Stewart, D. R. M. 2003. Evolution of Neogene globorotaliid foraminifera and Miocene

639   climate change, PhD Thesis. University of Bristol, Department of Earth Sciences.

640   Voje, K. L., T. F. Hansen, C. K. Egset, G. H. Bolstad, and C. Pelabon. 2014. Allometric

641   constraints and the evolution of allometry. Evolution 68:866-885.

642   Wei, K.-Y. 1994a. Allometric heterochrony in the Pliocene-Pleistocene planktic

643   foraminiferal clade *Globoconella*. Paleobiology 20:66-84.

644   —. 1994b. Stratophenetic tracing of phylogeny using SIMCA pattern recognition

645   technique: a case study of the Late Neogene planktic foraminifera *Globoconella*

646   clade. Paleobiology 20:52-65.

647

648

Figure captions

650   **Figure 1**

651   Analysed traits on foraminifera shells. Specimens were imaged in edge view (left), and

652   area, height and width were measured on the 2-dimensional shell representation

653   (right).

654

655   Figure 2

656   Box and whisker plots of A) shape and B) size of *Truncorotalia crassaformis* and C)

657   shape and D) size of *Globoconella puncticulata* at Site U1313 over time. E) and F)

658   represent the global oxygen isotope benthic stack (Lisiecki & Raymo, 2004) for the

659   study interval and the past 5 million years respectively, with key Marine Isotope Stages

660   shown in E).

661

662   Figure 3

663   Schematic of (A) the angle θ between $\mathbf{p_{max}}$ at time *t* and the direction of evolutionary

664   divergence (**z**) from the sample mean at time *t* to the sample mean at *t+1*. Here $\mathbf{p_{max}}$

665   represents the within-population allometry. (B) Evolutionary allometries were defined

666   as $\mathbf{p_{max}}$ of the phenotypic variance-covariance matrix of the sample means, and do not

667   necessarily line up with the within-population allometries of individual samples.

668

669   Figure 4

670   Linear regressions of first differences of A) mean size and B) mean shape of *Globoconella*

671   *puncticulata* (red) and *Truncorotalia crassaformis* (blue) against first differences of the

672   global benthic $\delta^{18}O$ stack (Lisiecki and Raymo 2005). Correlations between traits and

673    $\delta^{18}O$ were not significant for either species (Linear Model, *p* = 0.61, R^2 = 0.0037 and *p* =

674   0.99, R^2 = $2.2*10^{-4}$ for size and shape of *G. puncticulata* and *p* = 0.64, R^2 = 0.0031 and *p* =

675   0.77, R^2 = 0.0012 for size and shape of for size and shape of *T. crassaformis*).
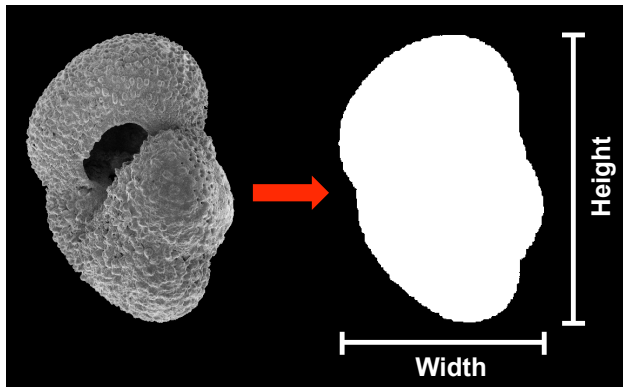
676

677   Figure 5

678   Sample means of size and shape for A) *Truncorotalia crassaformis* and B) *Globoconella*

679   *puncticulata* with colours indicating the climate phases (Initial Phase: red, Transition

680   Phase: yellow, Glacial Phase: blue). Within-population (dashed lines) and evolutionary

681   allometries within climate phases (coloured solid lines) and over the entire study

682   interval (solid black line) for C) *T. crassaformis* and D) *G. puncticulata*. In both species

683   short-term evolutionary allometries are significantly different from the long-term

684   evolutionary allometries (ANOVA, $p<0.001$ for both species). Angles between predicted

685   ($\mathbf{p_{max}}$) and observed ($\mathbf{z}$) one-step evolutionary change for E) *T. crassaformis* and F) *G.*

686   *puncticulata*. Dashed lines indicate the expected frequency of angles when drawn from a

687   random distribution. Angles are significantly smaller than expected from a random

688   distribution for both species (Wilcoxon rank sum test, $p<0.01$ for both species, see Table

689   4 for phase-specific p-values).

690

691

692

Figures
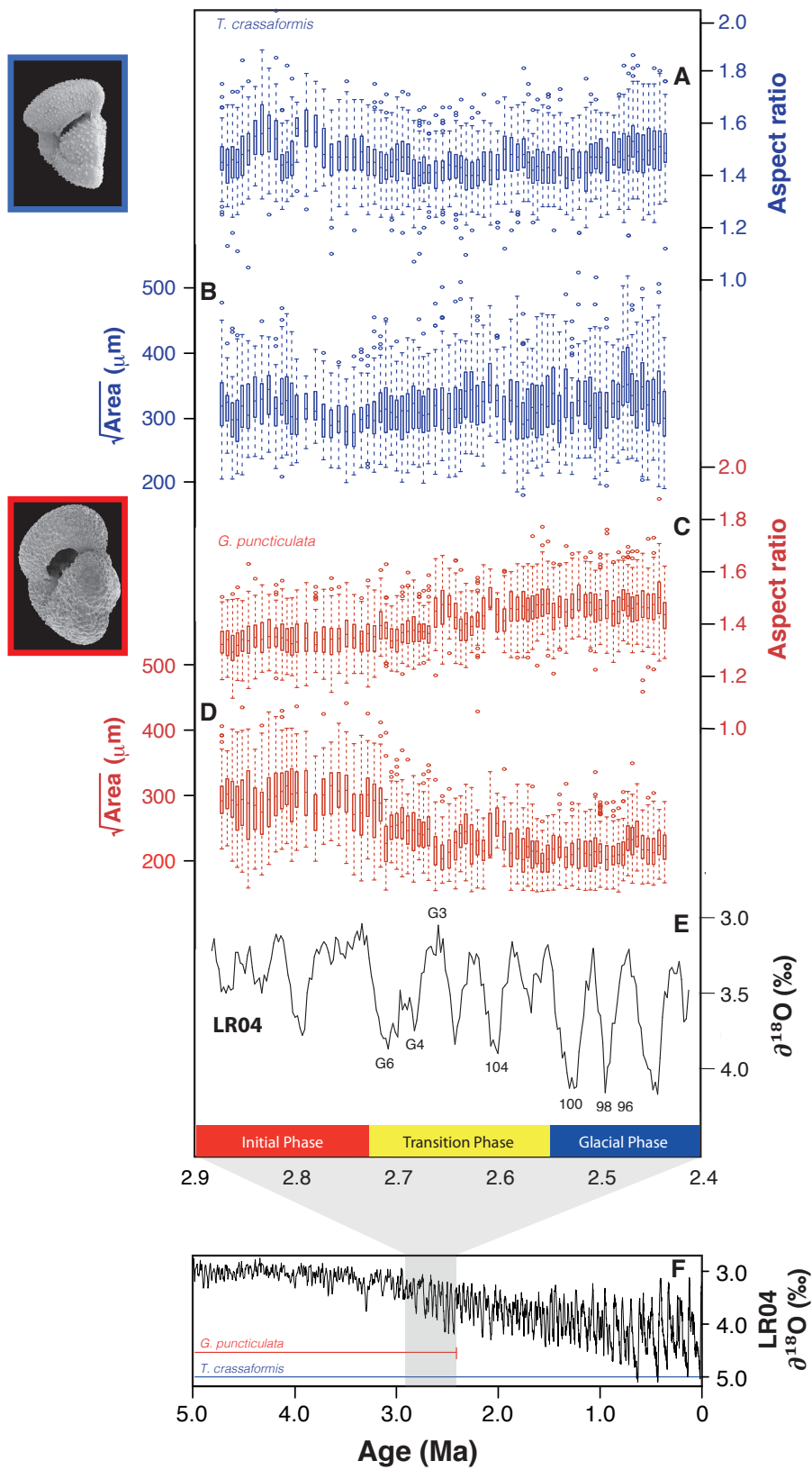

694

Figure 1

696

697

698

T. crassaformis

A — Aspect ratio (2.0, 1.8, 1.6, 1.4, 1.2, 1.0)

B — √Area (μm) (500, 400, 300, 200)

G. puncticulata

C — Aspect ratio (2.0, 1.8, 1.6, 1.4, 1.2, 1.0)

D — √Area (μm) (500, 400, 300, 200)

E — ∂¹⁸O (‰) (3.0, 3.5, 4.0)

G3
LR04
G6 G4   104
100 98 96

| Initial Phase | Transition Phase | Glacial Phase |

2.9   2.8   2.7   2.6   2.5   2.4

F — LR04 ∂¹⁸O (‰) (3.0, 4.0, 5.0)

G. puncticulata
T. crassaformis

5.0   4.0   3.0   2.0   1.0   0

Age (Ma)

699

Figure 2

701

31
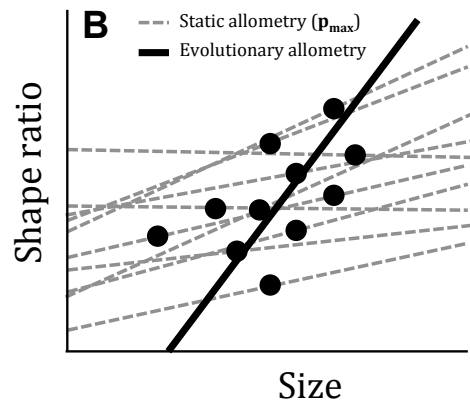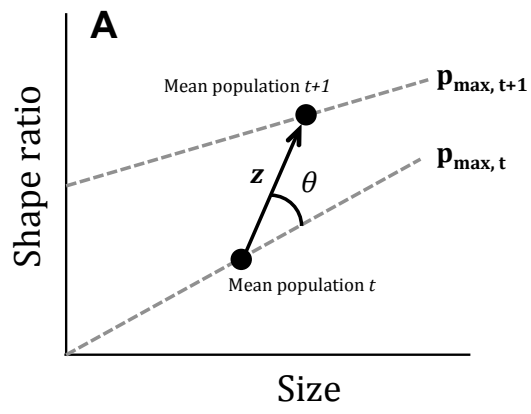
Figure 3

702

703

704   **Figure 4**

T. crassaformis

G. puncticulata

Initial Phase
Transition Phase
Glacial Phase

Static allometry
Evolutionary allometry (phase)
Evolutionary allometry (all)

Angle θ between observed and predicted change (radians)
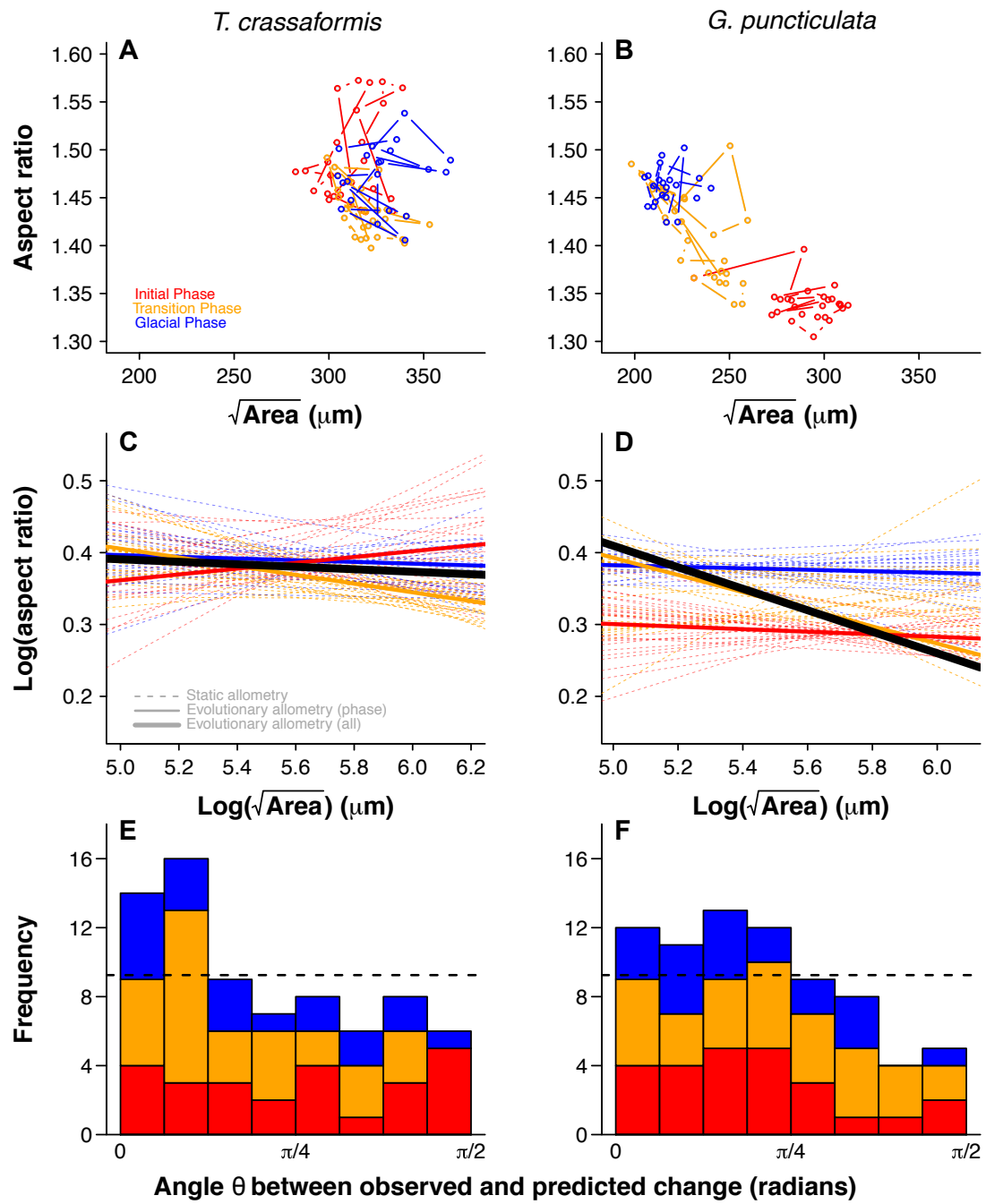
705

706   **Figure 5**

707

34

708

Tables

Table 1 AICc values and Akaike weights for stasis, unbiased random walks and directional evolution in size and shape of *Globoconella puncticulata* and *Truncorotalia crassaformis* over both the separate climate phases and the entire studied interval, analysed using the PaleoTS package in R.

Species	Trait	Phase	Stasis		Unbiased random walk		Directional evolution	
			AICc	Akaike weight	AICc	Akaike weight	AICc	Akaike weight
G. puncticulata	Size	Initial	194.0	0.532	194.8	0.359	197.2	0.109
		Transition	252.1	0.000	235.9	0.740	238.0	0.260
		Glacial	144.3	0.122	140.8	0.683	143.3	0.194
		All	**743.7**	**0.000**	**602.9**	**0.685**	**604.5**	**0.315**
	Shape	Initial	-141.3	0.963	-134.0	0.026	-132.3	0.011
		Transition	-91.2	0.000	-121.7	0.735	-119.7	0.265
		Glacial	-98.4	1.000	-80.8	0.000	-78.3	0.000
		All	**-205.5**	**0.000**	**-334.4**	**0.712**	**-332.6**	**0.288**
T. crassaformis	Size	Initial	202.2	0.006	192.5	0.763	194.9	0.231
		Transition	229.7	0.399	229.5	0.454	231.7	0.147
		Glacial	166.9	0.945	173.1	0.043	175.6	0.012
		All	**623.3**	**0.245**	**621.7**	**0.559**	**623.8**	**0.195**
	Shape	Initial	-74.0	0.002	-86.1	0.756	-83.8	0.242
		Transition	-126.9	0.046	-132.4	0.726	-130.1	0.228
		Glacial	-72.5	0.030	-78.9	0.753	-76.4	0.217
		All	**-251.5**	**0.000**	**-307.3**	**0.742**	**-305.2**	**0.258**

714

Table 2 Values for Lynch's delta metric for *Globoconella puncticulata* and *Truncorotalia crassaformis* size and shape. All values are less than 5% of the threshold proposed by Lynch (1990) to represent neutral evolution.

	Neutral evolution	*G. puncticulata*		*T. crassaformis*	
		Size	**Shape**	**Size**	**Shape**
Lynch's delta	$10^{-3} - 10^{-5}$	$1.28*10^{-7}$	$1.98*10^{-7}$	$1.21*10^{-6}$	$8.18*10^{-8}$

718

719

720

721

722 **Table 3** Linear Model results on evolutionary allometries over the entire interval with

723 ("Total interval with phases") and without phase-specific allometries ("Total interval").

724 R^2 values represent the variance explained in the total dataset by the model and p-values

725 represent the significance of the slopes.

Model	Species	Phase	R^2 model	p slopes
Total interval	*T. crassaformis*		0.0015	<0.01
	G. puncticulata		0.198	<0.001
Total interval with phases	*T. crassaformis*	Initial		<0.001
		Transition	0.067	<0.001
		Glacial		<0.001
	G. puncticulata	Initial		0.245
		Transition	0.336	<0.001
		Glacial		<0.01

726

727 **Table 4.** p-values of the Wilcoxon rank-sum test performed on the angles θ of both

728 *Globoconella* puncticulata and *T. crassaformis* and a set of randomly generated vectors.

Species	Phase	p-value (Wilcoxon rank sum test)
G. puncticulata	Initial	0.037
	Transition	0.283
	Glacial	0.020
	All	**0.007**
T. crassaformis	Initial	0.582
	Transition	0.003
	Glacial	0.020
	All	**0.003**

729